Supporting Information

Electron-Deficient $Pt_2M_2Pt_2$ Hexanuclear Metal Strings (M = Pt, Pd) Supported by Triphosphine Ligands

Eri Goto, Rowshan Ara Begum, Chiaki Ueno, Aya Hosokawa, Chie Yamamoto, Kanako Nakamae, Bunsho Kure, Takayuki Nakajima, Takashi Kajiwara, and Tomoaki Tanase*

Department of Chemistry, Faculty of Science, Nara Women's University, Kitauoya-nishi-machi, Nara 630-8506, Japan

Figure S6. (a) Results of single point DFT calculation by B3LYP/LANL2DZ methods for the crystal structure of $[Pt_6(\mu\text{–dpmp})_4(XylNC)_2]^{4+}$ (**7**), and (b) diagrams of the essential σ–MOs.

Figure S7. (a) Results of single point DFT calculation by B3LYP/LANL2DZ methods for the crystal structure of $[Pt_2Pd_2Pt_2(\mu\text{–dpmp})_4(XylNC)_2]^{4+}$ (**8**), and (b) diagrams of the essential σ–MOs.

Figure S8. UV-vis spectral changes for the titrations of (a) **7** and (b) **8** with successive addition of 0.1 equiv. of XylNC in dichloromethane.

Figure S9. UV-vis spectra of **10** and **11** in dichloromethane.

Figure S10. $^{31}P\{^1H\}$ NMR spectra (121 MHz) of (a) **10**, (b) **11**, and (c) **12a** in CD_2Cl_2 at room temperature.

Figure S11. ESI mass spectra of (a) **10**, (b) **11**, (c) **12a**, and (d) **13a** in CH_2Cl_2 at room temperature.

Figure S12. (a) UV-vis spectral changes in dichloromethane for the titration of **7** by successive addition of dppe (portions of 0.2 equiv.) up to a total amount of 2.0 equivs. (b) The spectral changes with adding dppe from 0 to 1 equiv. amounts, and (c) those from 1 to 2 equiv. amounts.

Figure S13. Perspective view for the complex cation of **14a** with atomic numbering schemes.

Figure S14. $^{31}P\{^1H\}$ NMR spectra for the Au-bound PPh_3 peaks of (a) **15** and (b) **16**.

Figure S15. ESI mass spectra of (a) **15** and (b) **16** in CH_2Cl_2 at room temperature

Figure S16. A perspective view for the complex cation of **16** with atomic numbering schemes.

Table S1. Results of DFT Calculations on $[Pt_2M_2Pt_2(\mu\text{-dpmp})_2(XylNC)_2](PF_6)_4$ (M = Pt (**7**), Pd (**8**)) and $[Pt_2M_2Pt_2(\mu\text{-H})(\mu\text{-dpmp})_2(XylNC)_2](PF_6)_3$ (M = Pt (**2**), Pd (**3**)) and Their Model Complexes **M7**, **M8**, and **M2**.[a]

Compound	**M2** [b]	**2** [b]	**3** [b]	**M7** [c]	**M8** [c]	**7** [c]	**8** [c]
Methods[a]	opt[d]	sp[e]	sp[e]	opt[d]	opt[d]	sp[e]	sp[e]
M_{cen}	Pt	Pt	Pd	Pt	Pd	Pt	Pd
Structural Parameters							
av. Pt_{out}-Pt_{inn}, Å	2.798	2.7156	2.7136	2.790	2.769	2.701	2.687
av. Pt_{inn}-M_{cen}, Å	2.858	2.7370	2.7562	2.979	3.023	2.800	2.787
M_{cent}-M_{cent}, Å	3.526	3.3093	3.2514	3.042	3.138	2.823	2.834
av. M_{cen}-H_b, Å	1.763	1.655	1.626	-	-	-	-
av. Pt_{out}-C, Å	2.036	1.968	1.953	2.010	2.004	1.953	1.922
M_{cen}-H_b-M_{cen}, °	178.92	180.00	180.00	-	-	-	-
Natural Charge							
Pt_{out}	-0.47	-0.36	-0.35	-0.32	-0.32	-0.22	-0.20
Pt_{inn}	-0.44	-0.47	-0.48	-0.31	-0.32	-0.46	-0.47
M_{cen}	-0.42	-0.40	-0.25	-0.40	-0.19	-0.57	-0.40
H_b	-0.11	-0.24	-0.25	-	-	-	-
C	+0.35	+0.25	+0.24	+0.35	+0.35	+0.26	+0.25
	*C*NMe	*C*NXyl	*C*NXyl	*C*NMe	*C*NMe	*C*NXyl	*C*NXyl
Wiberg Bond Indices							
av. Pt_{out}-Pt_{inn}	0.424	0.387	0.376	0.538	0.548	0.467	0.465
av. Pt_{inn}-M_{cen}	0.416	0.343	0.290	0.308	0.275	0.281	0.248
M_{cen}-M_{cen}	0.084	0.112	0.100	0.202	0.144	0.223	0.159
av. M_{cen}-H_b	0.365	0.261	0.240	-	-	-	-
av. Pt_{out}-C	0.781	0.617	0.627	0.778	0.786	0.584	0.624

[a] DFT calculations were carried out by *Gaussian03* program package with B3LYP functionals and LANL2DZ basis set. [b] See ref. 10b. [c] This work. [d] Optimization of the structures. [e] Single point SCF calculations on the structure determined by X-ray crystallography.

Table S2. Crystallographic Data of Complexes **7**·3CH_2Cl_2 and **8**·5CH_2Cl_2

Compound	**7**·3CH_2Cl_2	**8**·5CH_2Cl_2
formula	$C_{149}H_{140}N_2Cl_6$-$F_{24}P_{16}Pt_6$	$C_{151}H_{144}N_2Cl_{10}$-$F_{24}P_{16}Pt_4Pd_2$
formula wt	4293.56	4286.04
cryst. syst	orthorhombic	orthorhombic
space group	$C222_1$	$C222_1$
a, Å	26.364(7)	26.4070(9)
b, Å	40.635(11)	40.5880(13)
c, Å	41.437(10)	41.3526(13)
α, deg	90	90
β, deg	90	90
γ, deg	90	90
V, Å^3	44391(20)	44322(2)
Z	8	8
temp, °C	-120	-120
D_{calcd}, g cm^{-1}	1.285	1.285
μ, mm^{-1} (Mo Kα)	3.995	2.956
2θ range, deg	6–55	6–55
R_{int}	0.081	0.058
no. of reflns collected	211560	209415
no. of unique reflns	50423	50468
no. of obsd reflns ($I > 2\sigma(I)$)	36375	42759
no. of variables	1837	1866
$R1$[a]	0.073	0.089
$wR2$[b]	0.222	0.249
GOF	1.021	1.075

[a] $R1 = \Sigma \| |F_o| - |F_c| | / \Sigma |F_o|$ (for obsd. refs with $I > 2\sigma(I)$). [b] $wR2 = [\Sigma w(F_o^2 - F_c^2)^2 / \Sigma w(F_o^2)^2]^{1/2}$ (for all refs).

Table S3. Crystallographic Data of Complexes **14a**·6CH_2Cl_2, **15**·3.5CH_2Cl_2, and **16**·3CH_2Cl_2

Compound	**14a**·6CH_2Cl_2	**15**·3.5CH_2Cl_2	**16**·3CH_2Cl_2
formula	$C_{122}H_{114}Cl_{12}F_{12}P_{12}Pt_3$	$C_{94.5}H_{89}NCl_8F_{12}P_9Pt_3Au$	$C_{94}H_{88}NCl_7F_{12}P_9Pt_2PdAu$
formula wt	3190.61	2811.35	2680.20
cryst. syst	triclinic	monoclinic	monoclinic
space group	*P*-1	$P2_1/c$	$P2_1/c$
a, Å	13.203(4)	16.4325(11)	16.2983(17)
b, Å	13.902(5)	23.6825(15)	23.534(2)
c, Å	18.468(6)	27.6089(19)	27.456(3)
α, deg	85.707(9)		
β, deg	69.334(6)	96.145(3)	96.399(5)
γ, deg	85.233(9)		
V, Å^3	3156.9(17)	10682.6(12)	10465.5(18)
Z	1	4	4
temp, °C	-120	-120	-120
D_{calcd}, g cm^{-1}	1.678	1.748	1.701
μ, mm^{-1} (Mo Kα)	3.773	5.673	4.606
2θ range, deg	6–55	6–55	6–55
R_{int}	0.056	0.065	0.060
no. of reflns collected	29041	55985	57415
no. of unique reflns	13744	23620	23401
no. of obsd reflns ($I > 2\sigma(I)$)	9891	14493	14666
no. of variables	737	1253	1208
*R*1[a]	0.085	0.081	0.097
*wR*2[b]	0.209	0.239	0.265
GOF	1.074	1.093	1.030

[a] $R1 = \Sigma \big| |F_o| - |F_c| \big| / \Sigma |F_o|$ (for obsd. refs with $I > 2\sigma(I)$). [b] $wR2 = [\Sigma w(F_o^2 - F_c^2)^2 / \Sigma w(F_o^2)^2]^{1/2}$ (for all refs).

Figure S1. $^{31}P\{^{1}H\}$ NMR spectra (121 MHz) of (a) **7** (M = Pt) in acetone-d_6 and (b) **8** (M = Pd) in CD_2Cl_2 at room temperature and the assignments.

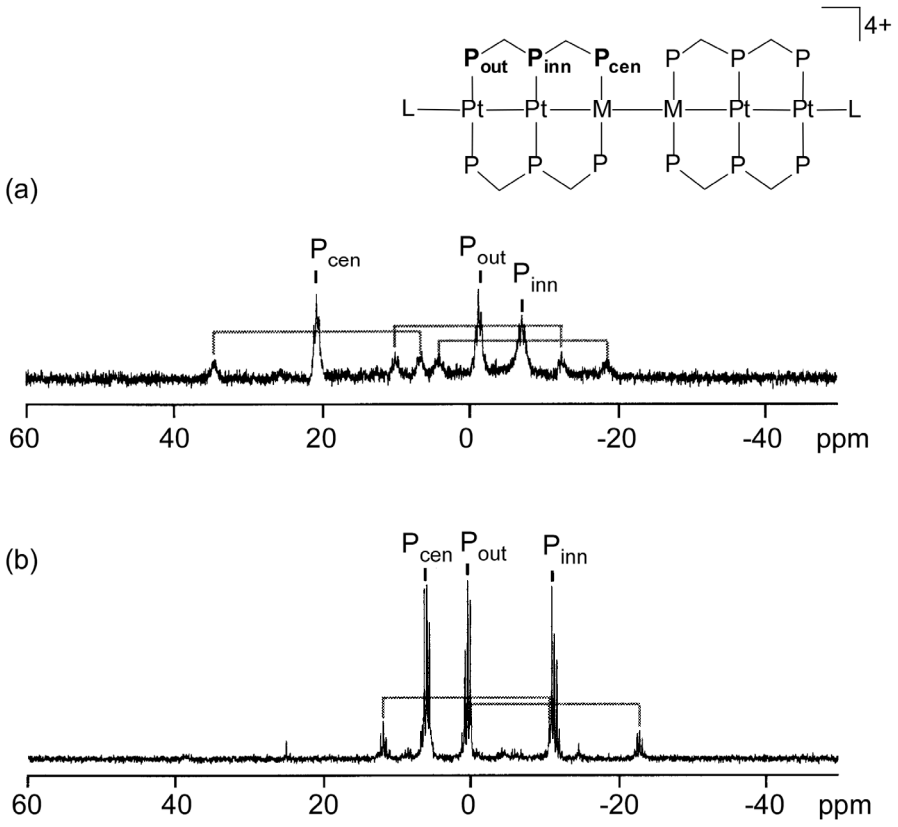

Figure S2. ESI mass spectra of (a) **7** (M = Pt) and (b) **8** (M = Pd) in acetone at room temperature and the observed and simulated spectra for $[Pt_2M(dpmp)_2(XylNC)]^{2+}$ at *m/z* = 864.635 (**7**) and 820.107 (**8**).

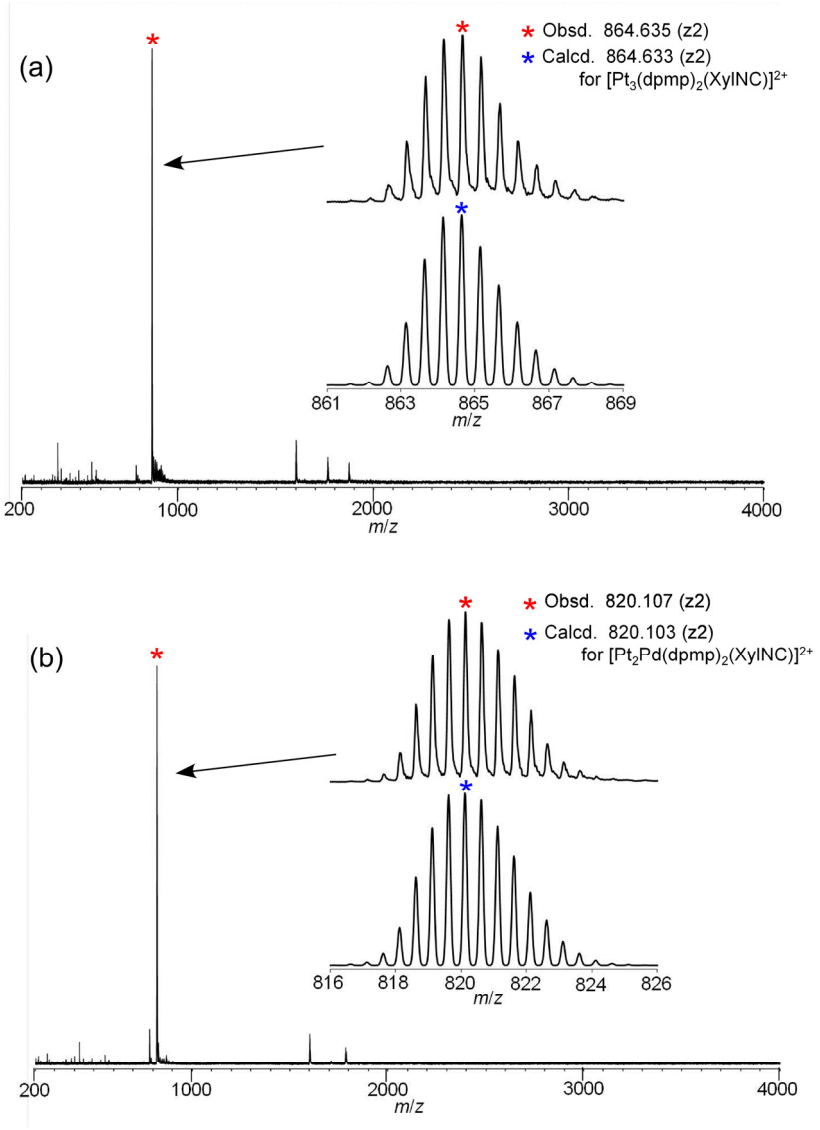

Figure S3. Perspective drawings for the cluster cation of (a) **8A** and (b) **8B** with atomic numbering schemes. The Pt, Pd, and P atoms are illustrated with thermal ellipsoids at 40% probability level. The hydrogen atoms are omitted and the C and N atoms are drawn with arbitrary spherical model for clarity. Pt (yellow), Pd (green), P (pink), N (blue), and C (gray).

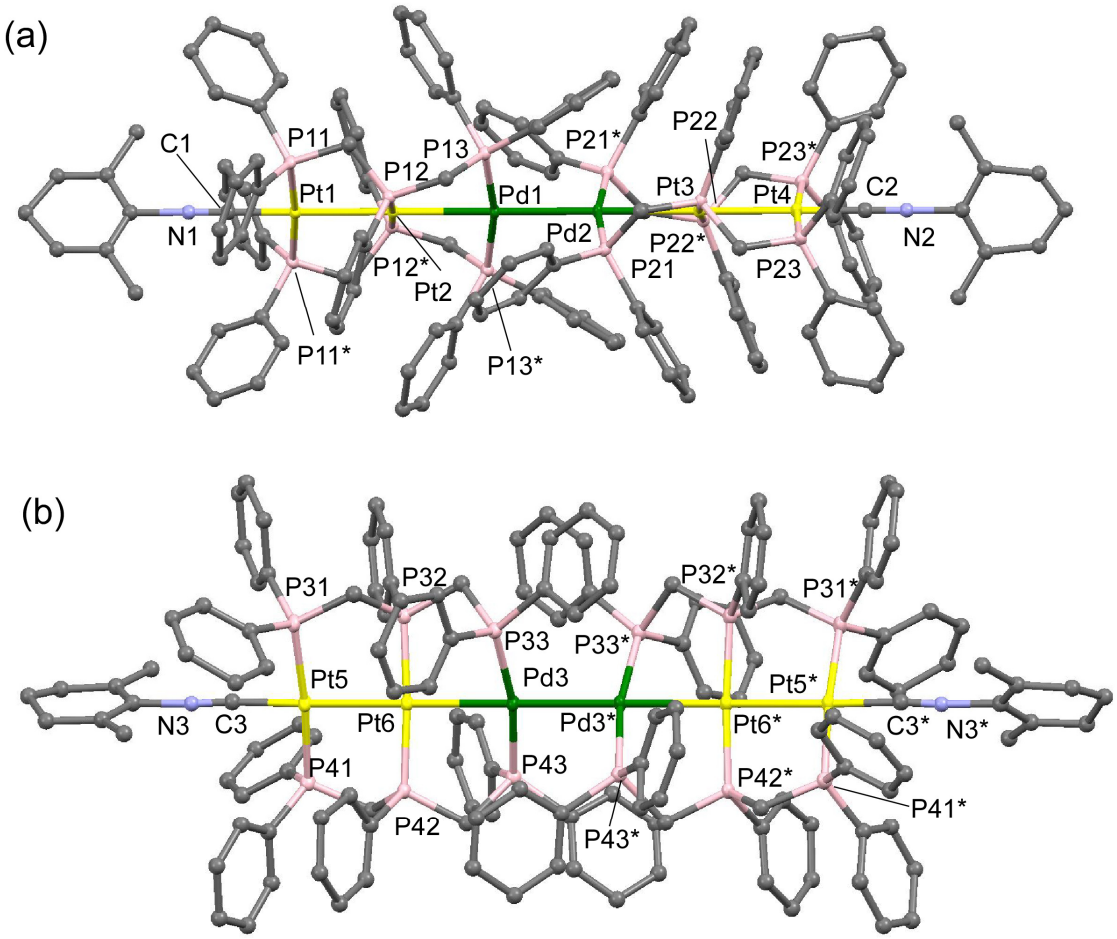

Figure S4. (a) DFT optimized structure of the model complex $[Pt_6(C_2H_9P_3)_4(CH_3NC)_2]^{4+}$ (**M7**) with B3LYP/LANL2DZ level and the results of natural population analyses. (b) Diagrams of the essential σ–MOs.

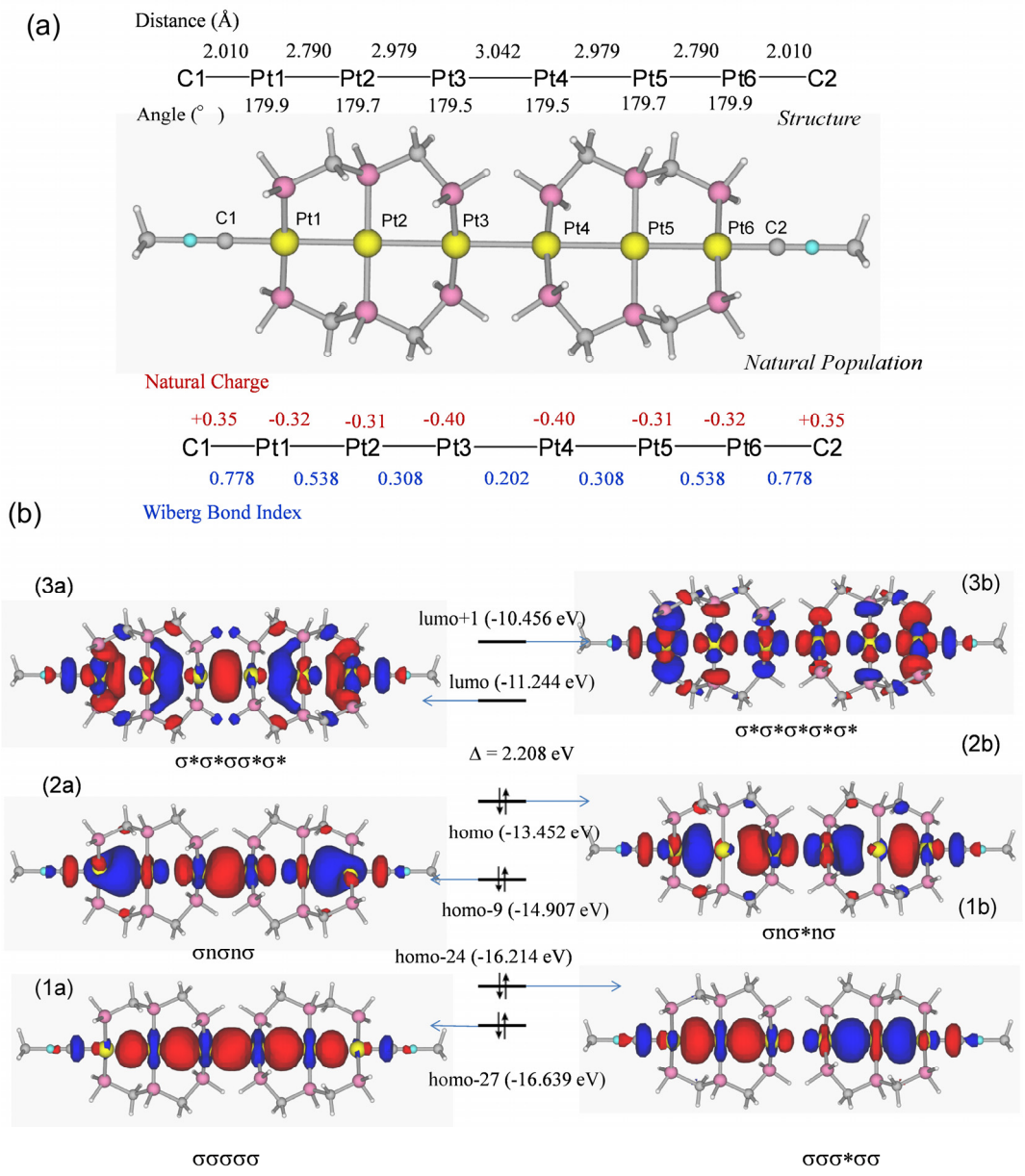

Figure S5. DFT optimized structure of the model complex $[Pt_2Pd_2Pt_2(C_2H_9P_3)_4(CH_3NC)_2]^{4+}$ (**M8**) with B3LYP/LANL2DZ level and the results of natural population analyses. (b) Diagrams of the essential σ–MOs.

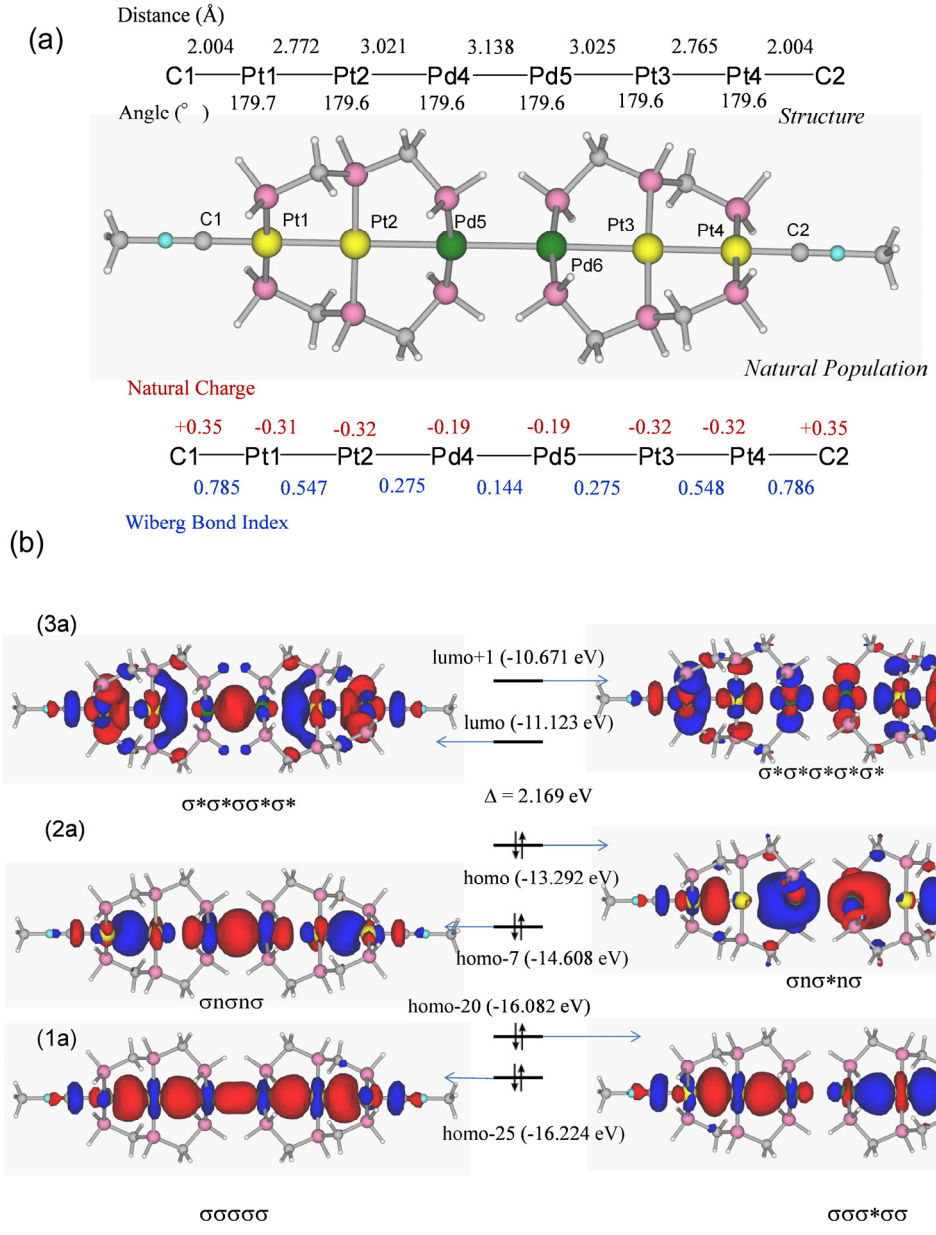

Figure S6. (a) Results of single point DFT calculation by B3LYP/LANL2DZ methods for the crystal structure of $[Pt_6(\mu\text{–dpmp})_4(XylNC)_2]^{4+}$ (**7**), and (b) diagrams of the essential σ–MOs.

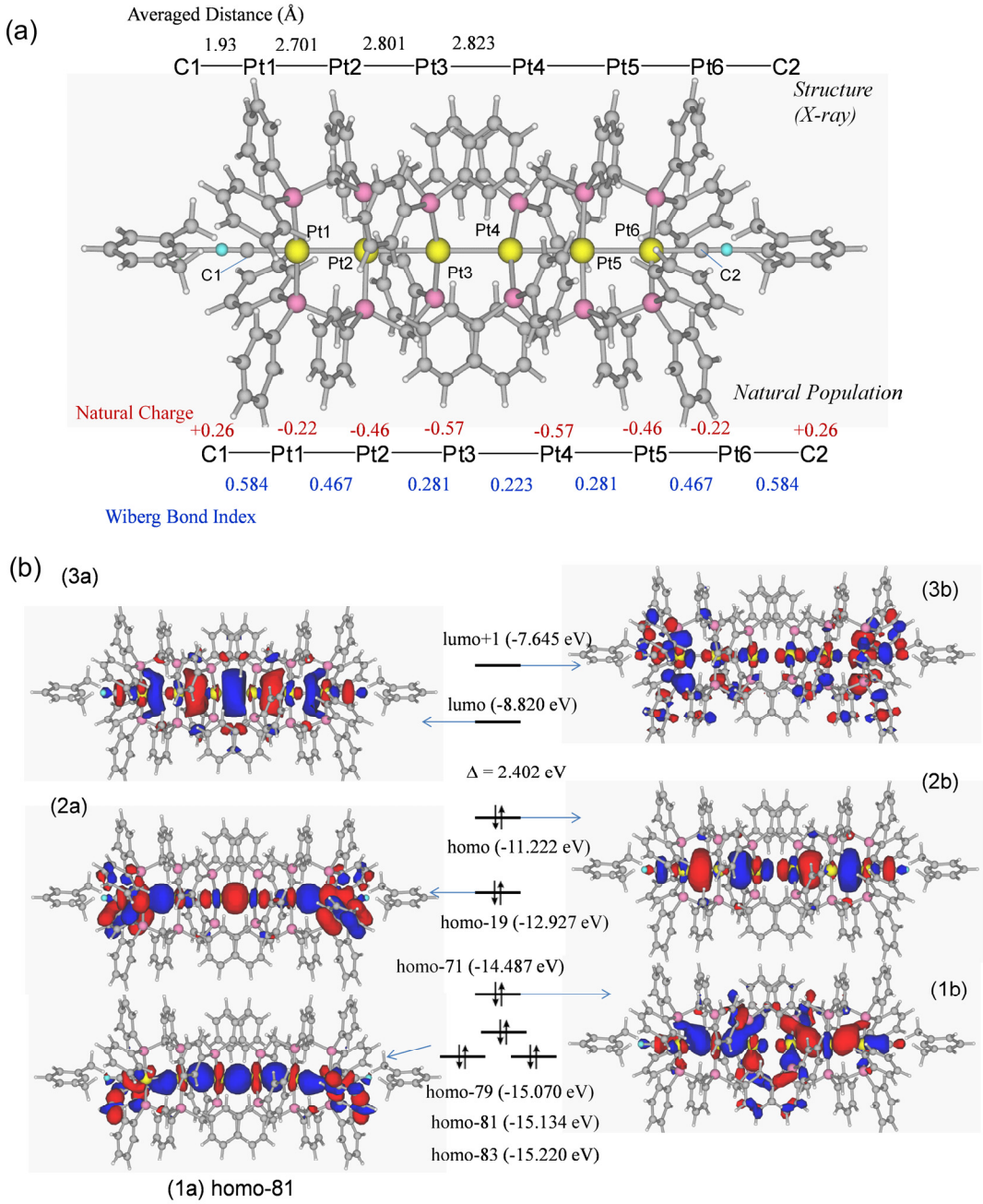

Figure S7. (a) Results of single point DFT calculation by B3LYP/LANL2DZ methods for the crystal structure of $[Pt_2Pd_2Pt_2(\mu\text{–dpmp})_4(XylNC)_2]^{4+}$ (**8**), and (b) diagrams of the essential σ–MOs.

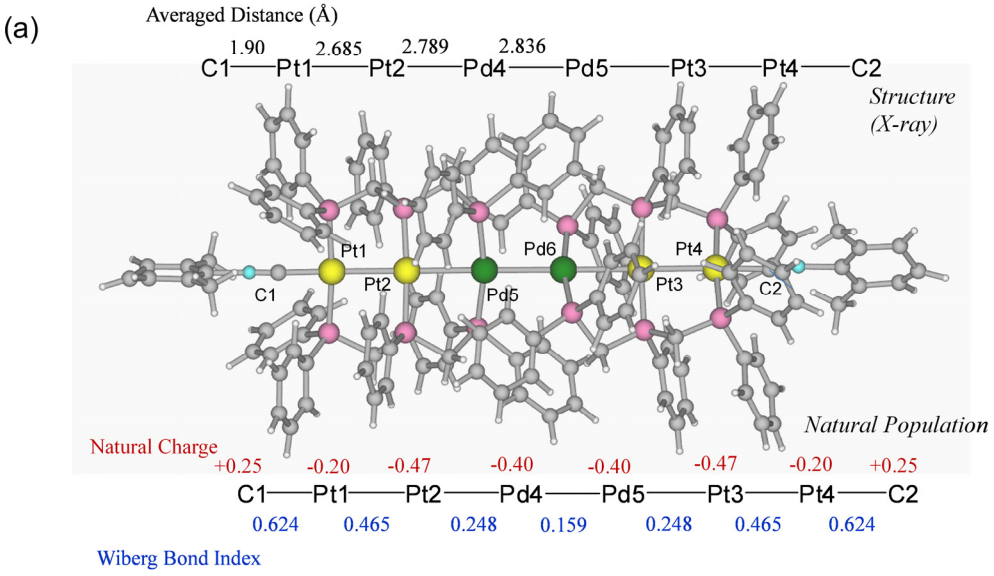

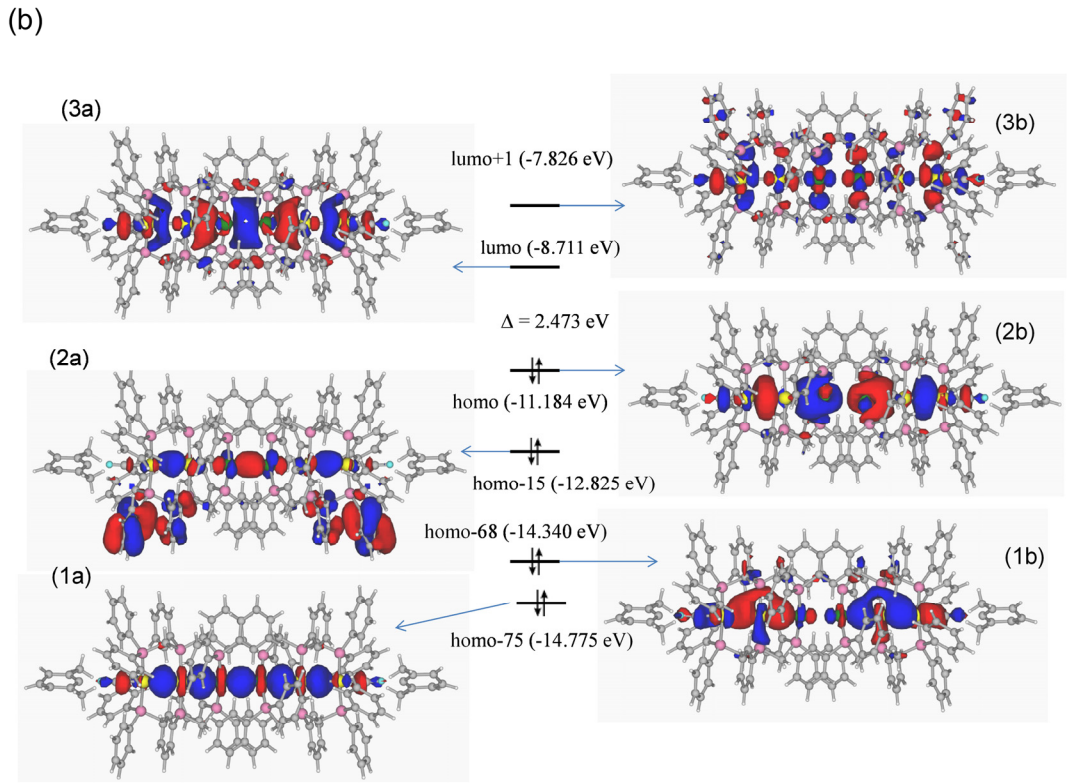

Figure S8. UV-vis spectral changes for the titrations of (a) **7** and (b) **8** with successive addition of 0.1 equiv. of XylNC in dichloromethane.

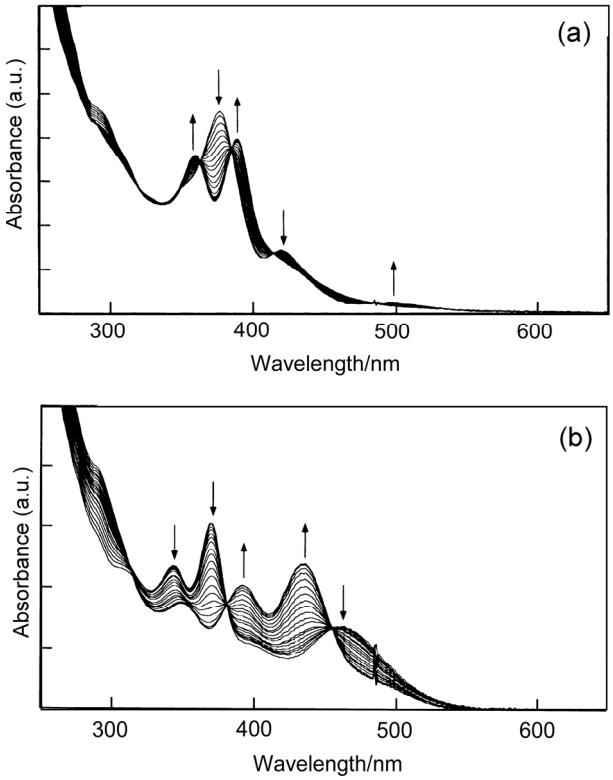

Figure S9. UV-vis spectra of **10** and **11** in dichloromethane.

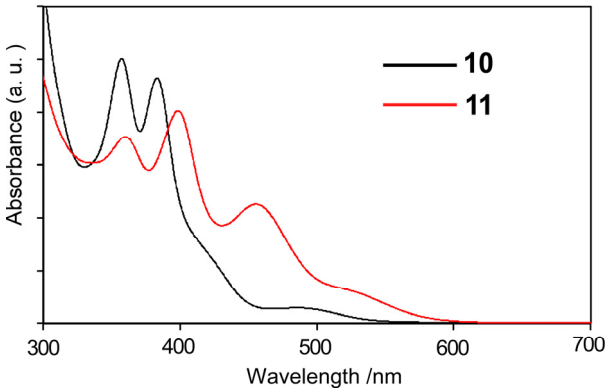

Figure S10. $^{31}P\{^{1}H\}$ NMR spectra (121 MHz) of (a) **10**, (b) **11**, and (c) **13a** in CD_2Cl_2 at room temperature.

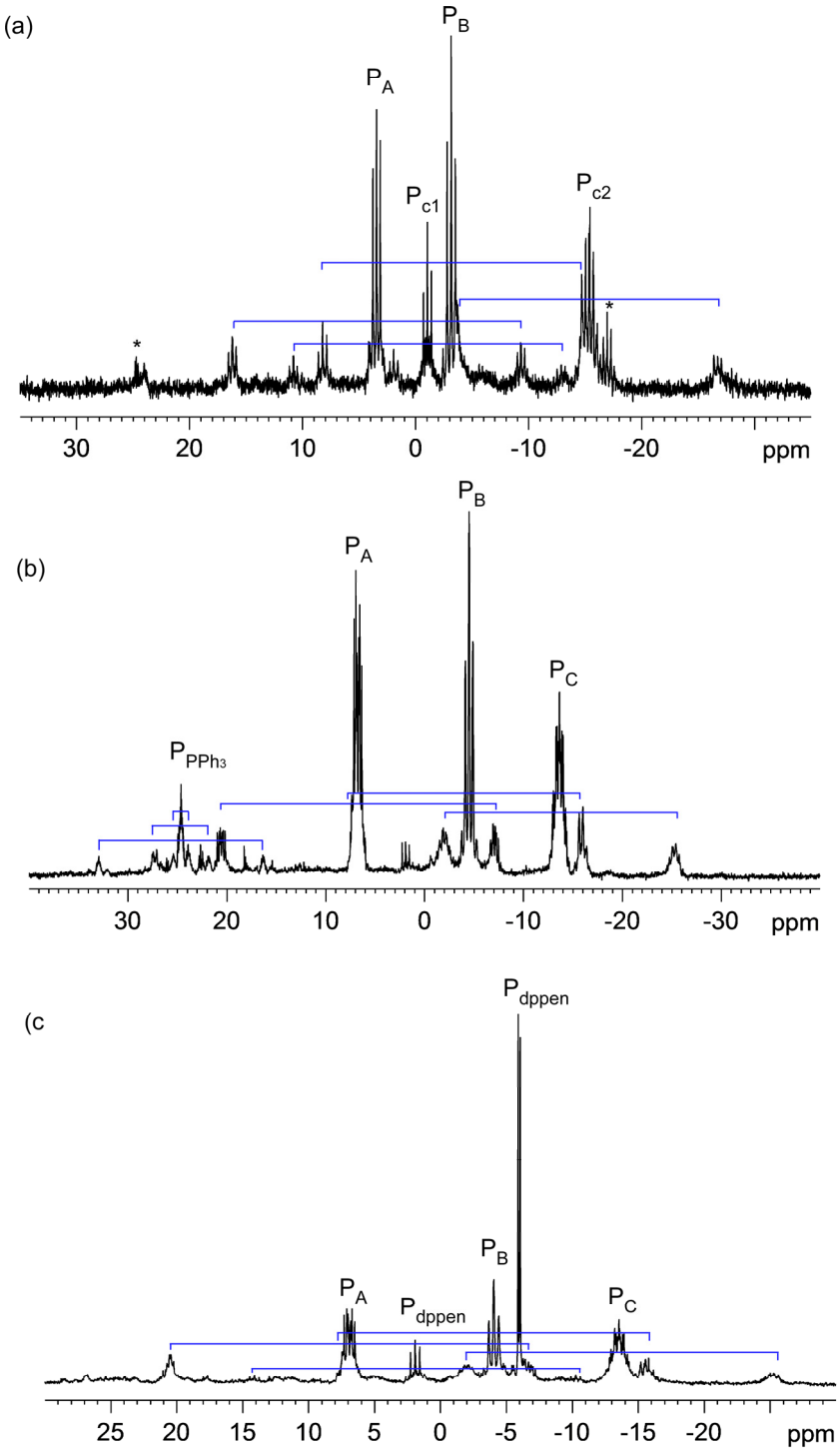

Figure S11. ESI mass spectra of (a) **10**, (b) **11**, (c) **12a**, and (d) **13a** in CH_2Cl_2 at room temperature.

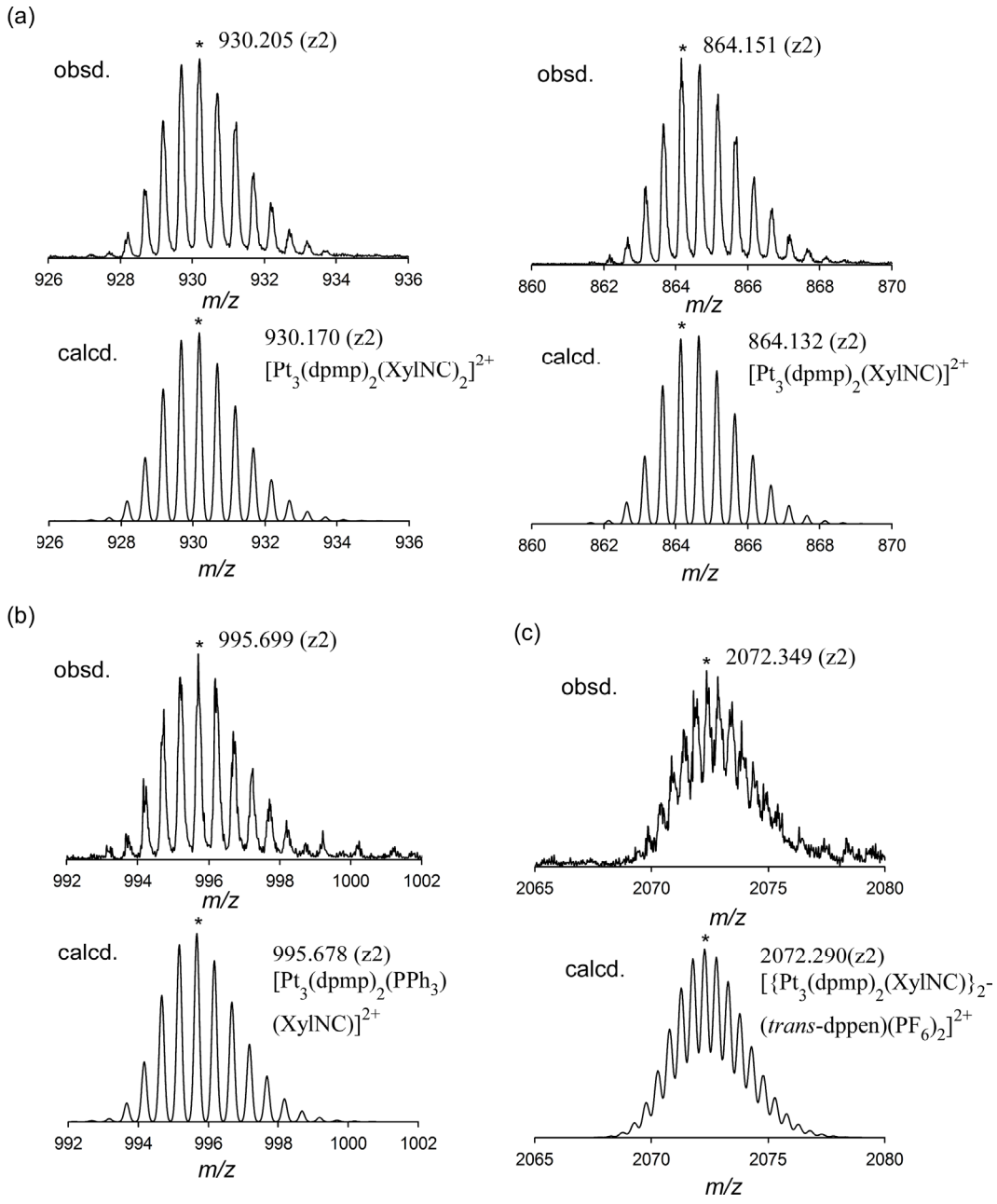

(d)

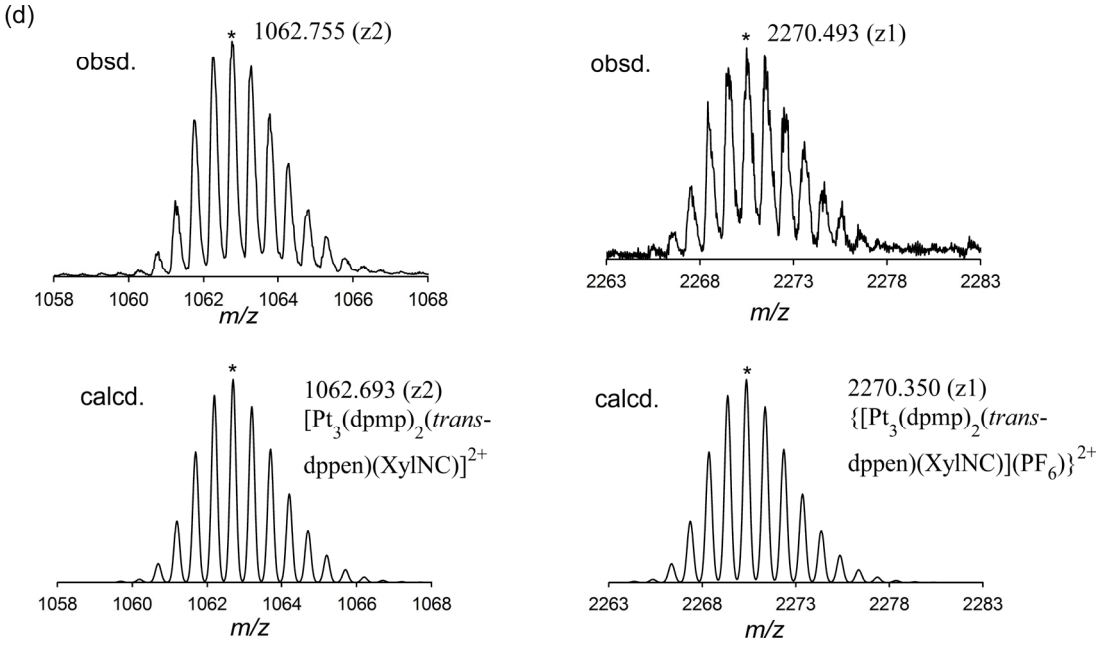
obsd.
1062.755 (z2)
1058
1060
1062
1064
1066
1068
m/z
obsd.
2270.493 (z1)
2263
2268
2273
2278
2283
m/z
calcd.
1062.693 (z2)
[Pt3(dpmp)2(trans-dppen)(XylNC)]2+
1058
1060
1062
1064
1066
1068
m/z
calcd.
2270.350 (z1)
{[Pt3(dpmp)2(trans-dppen)(XylNC)](PF6)}2+
2263
2268
2273
2278
2283
m/z

Figure S12. (a) UV-vis spectral changes in dichloromethane for the titration of **7** by successive addition of dppe (portions of 0.2 equiv.) up to a total amount of 2.0 equivs. (b) The spectral changes with adding dppe from 0 to 1 equiv. amounts, and (c) those from 1 to 2 equiv. amounts.

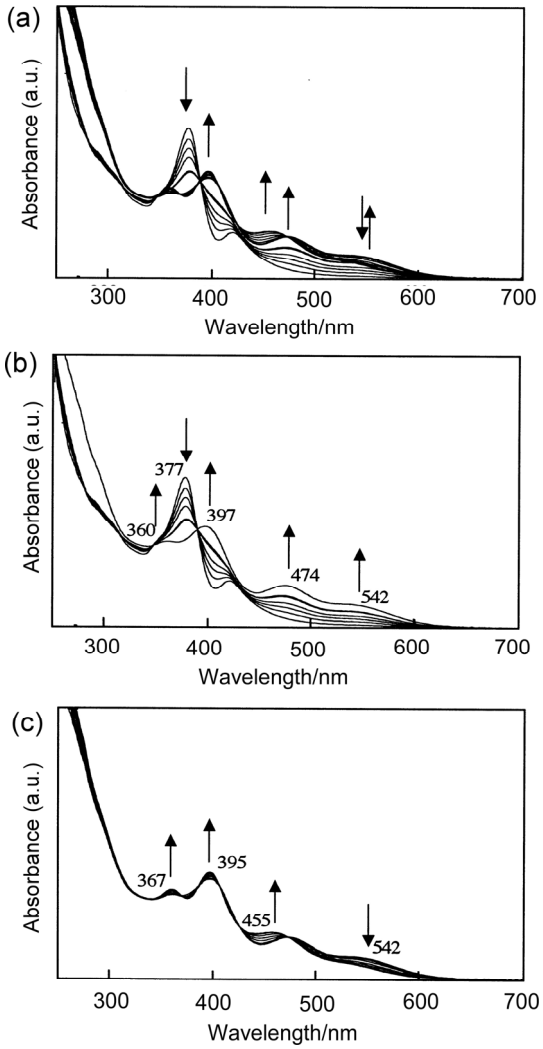

Figure S13. Perspective view for the complex cation of **14a** with atomic numbering schemes. The Pt and P atoms are illustrated with thermal ellipsoids at 40% probability level. The hydrogen atoms are omitted and the C atoms are drawn with arbitrary spherical model for clarity. Pt (yellow), P (pink), and C (gray).

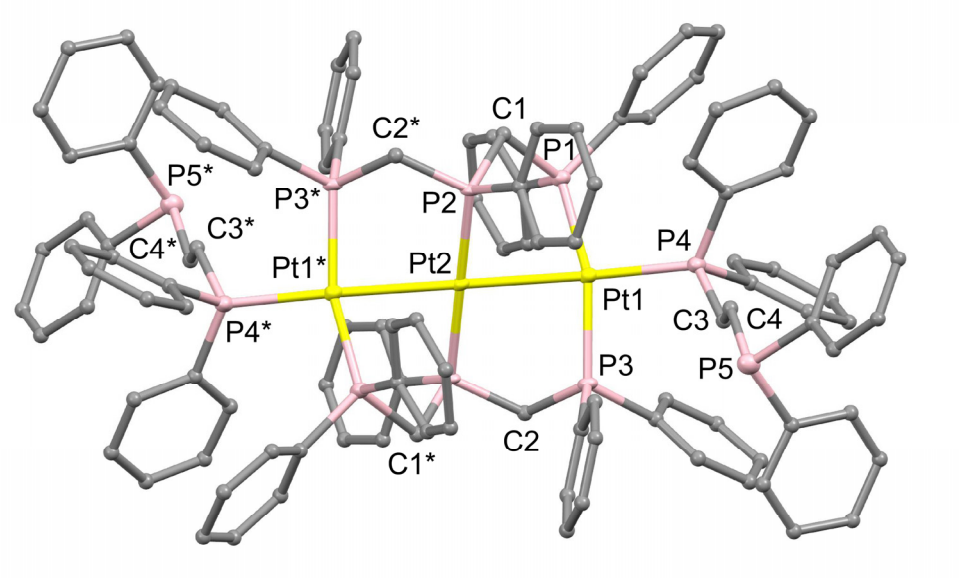

Figure S14. $^{31}P\{^{1}H\}$ NMR spectra for the Au-bound PPh_3 peaks of (a) **15** and (b) **16**. The peaks with asterisk are impurity.

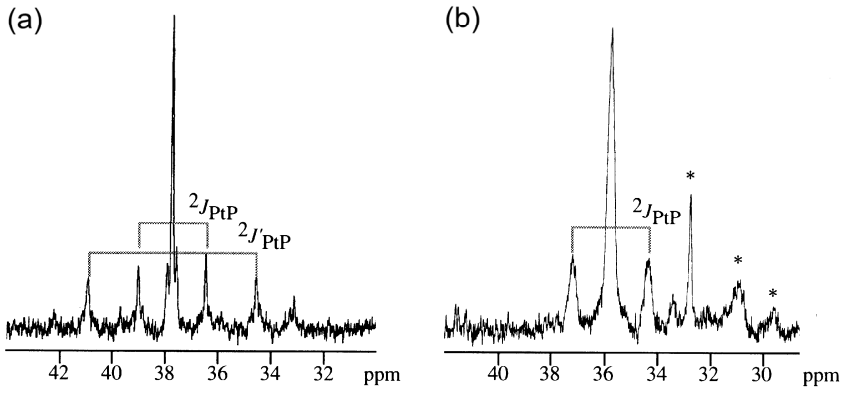

Figure S15. ESI mass spectra of (a) **15** and (b) **16** in CH_2Cl_2 at room temperature.

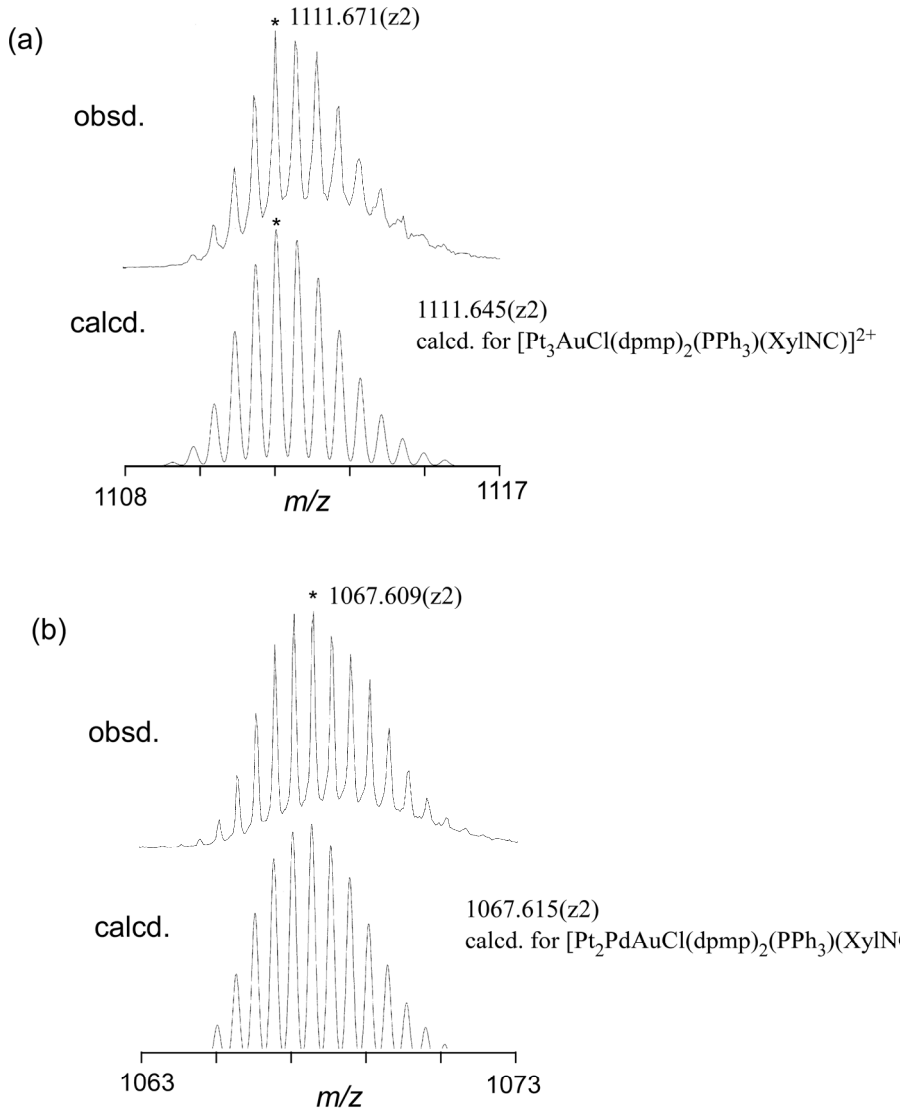

Figure S16. A perspective view for the complex cation of **16** with atomic numbering schemes. The Au, Pt, Pd, Cl, and P atoms are illustrated with thermal ellipsoids at 40% probability level. The hydrogen atoms are omitted and the C and N atoms are drawn with arbitrary spherical model for clarity. Au (violet), Pt (yellow), Pd (green), Cl (light green), P (pink), N (blue), and C (gray).